IEICE TRANS. COMMUN., VOL.E93–B, NO.10 OCTOBER 2010

INVITED PAPER *Special Section on Advanced Technologies in Antennas and Propagation in Conjunction with Main Topics of ISAP2009*

Bandwidth and Gain Enhancement of Microstrip Patch Antennas Using Reflective Metasurface

Sarawuth CHAIMOOL[†a)], ***Member***, **Kwok L. CHUNG**[††], ***Nonmember***, ***and*** **Prayoot AKKARAEKTHALIN**[†], ***Member***

SUMMARY Bandwidth and gain enhancement of microstrip patch antennas (MPAs) is proposed using reflective metasurface (RMS) as a superstrate. Two different types of the RMS, namely- the double split-ring resonator (DSR) and double closed-ring resonator (DCR) are separately investigated. The two antenna prototypes were manufactured, measured and compared. The experimental results confirm that the RMS loaded MPAs achieve high-gain as well as bandwidth improvement. The desinged antenna using the RMS as a superstrate has a high-gain of over 9.0 dBi and a wide impedance bandwidth of over 13%. The RMS is also utilized to achieve a thin antenna with a cavity height of 6 mm, which is equivalent to $\lambda/21$ at the center frequency of 2.45 GHz. At the same time, the cross polarization level and front-to-back ratio of these antennas are also examined.

key words: *wideband, high-gain, metamaterial, Fabry-Perot cavity (FPC), frequency selective surface (FSS)*

1. Introduction

Microstrip patch antennas (MPAs) offer many attractive features including small size, light weight, low profile, easy fabrication and planar structure. However, there are two major disadvantages associated with MPAs: low gain and narrow impedance bandwidth, which seriously limit their applications. Many wideband techniques for MPAs have been reported [1]. Furthermore, recent increases in the transmission and reception of information have created a need for wideband and high-gain antennas. Conventional way to obtain a high-gain antenna is formed an antenna array with appropriate feeding network. However, intricate feeding mechanisms to meet suitable phase delays make the antenna system complicated and also cause signal losses. Various techniques have been proposed to produce high directivity at broadside for MPAs and printed-circuit antennas [2], [3]. Amongst enhancement techniques, one of the effective methods that can significantly increase the antenna gain employs either high-relative permittivity ($\epsilon_r \gg 1$) or high-relative permeability ($\mu_r \gg 1$) superstrate as an antenna radome [3]. The superstrate acts as an aperture antenna and increases effective aperture size, and hence it enhances the directivity beyond that of the original primary antenna. A class of antennas that using a superstrate is also known as the resonant cavity antenna (RCA).

A subgroup of the family of RCAs that have attracted considerable interest is antennas with the partially reflective surface (PRS). These antennas are formed when an array of metallic periodic unit cells is suspended above a metallic ground plane. The PRS is generally realized using a planar periodic material (dipole or aperture). To realize the high directivity of an MPA, a commonly used method is to put the PRS on top of a metallic ground plane. The resulting antenna is a type of Fabry-Perot resonant cavity (FPC). There are several papers to design and analyze high-gain antennas based on FPC [4]–[6]. The FPC directive antenna was proposed with a single metallic grid [4]. As a result, it has very high directivity of about 600 at 14.8 GHz. However, it has a very narrow bandwidth (about 0.3%) due to its high quality factor, which limits its applications. Moreover, the distance between the PRS and the ground plane, which determines the resonant frequency, still needs to be about a half-wavelength ($\lambda/2$) of the resonant frequency. By replacing the conventional metallic ground plane with the high impedance surface (HIS) as an artificial magnetic conductor (AMC), these cavity heights have been reduced to about $\lambda/4$, while maintaining a high directivity [7], [8].

Another method of obtaining a directive antenna is to place a primary source inside metamaterials (MTMs). Recently, left-handed metamaterials (LH-MTMs) or double negative (DNG) materials have attracted lots of attention because of their unusual electromagnetic properties. In the last few years, the interest of MTMs not only may attain negative values, but also low and zero values in the certain frequency bands. Epsilon-near-zero (ENZ), mu-near-zero (MNZ) and zero refractive index (ZRI) materials have been proposed as MTMs to design several novel electromagnetic devices [9]. The use of MTM structures as superstrate of MPAs to achieve directivity enhancement has been presented [10], [11]. For this unique property, the high directivity antennas by applying the collimation effect of refractive near zero (RNZ) or ZRI have been proposed [10]–[12]. The refraction index (n) = 0 would occur at the frequencies where either $\mu_r = 0$ or $\epsilon_r = 0$.

By replacing a PRS with MTMs, which is designated as reflective metasurface (RMS), bandwidth and gain enhancement of MPAs using the RMS as a superstrate is proposed in this paper. The RMS exhibits the unusual properties of MNZ and high-epsilon (high-ϵ) medium. Accord-

Manuscript received March 12, 2010.
Manuscript revised June 1, 2010.

[†]The authors are with the Wireless Communication Research Group, Department of Electrical Engineering, Faculty of Engineering, King Mongkut's University of Technology North Bangkok, Bangkok, Thailand.
[††]The author is with the Department of Electronic and Information, Hong Kong Polytechnic University, Hong Kong.
a) E-mail: sarawuth@kmutnb.ac.th

DOI: 10.1587/transcom.E93.B.2496

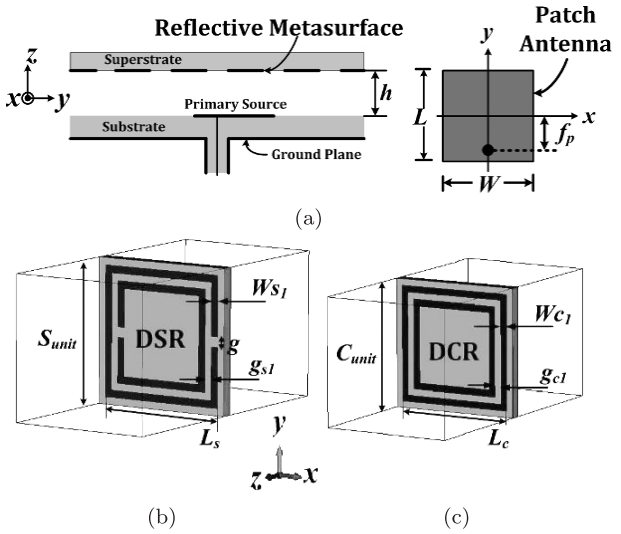

Fig. 1 (a) Configuration of a microstrip patch antenna with reflective metasurface (RMS) as a superstrate,(b) a unit cell of double split-ring resonator (DSR) and (c) a unit cell of double closed-ring resonator (DCR).

ing to our literature review, most FPC antennas are applied to the frequency in the X-band around 10 GHz, which have limited applications in practice. This study is subsequently extended to practical finite-size antenna designs operating at a wireless LAN (WLAN) frequency of 2.45 GHz. The configuration of the proposed antenna is shown in Fig. 1(a). It consists of the RMS on top an MPA. The RMS and the ground plane form a resonant cavity, whereas the MPA couples energy to the cavity in the near-field region. A cavity height of h is defined as the distance between the RMS and the MPA. The obtained impedance bandwidths and gains of different configurations are compared. In all the structures presented in this paper, an MPA having the same size as a primary source is used for the excitation. The characteristics of two RMS types will be discussed in Sect. 2. In Sect. 3, MPAs with use of the RMS are studied. Finally, the verification of simulated results is performed by experiments. Simulated results have been obtained using the IE3D [13] and the CST [14] softwares.

2. Reflective Metasurface Characteristics

In this paper, two different types of the RMS were employed during the research studies presented for the propose of comparison. We will consider the two simply structures, namely- double split-ring resonator (DSR) and double closed-ring resonator (DCR) as shown in Fig. 1(b) and Fig. 1(c), respectively. The DCR acting as a coupled closed-loop resonator is used for comparison with DSR, which acts as a coupled open-loop resonator. The physical parameters of the DSR are given in the unit of mm as follows: S_{unit} = 19.62, L_s = 18.43 and $W_{s1} = g_{s1} = g$ = 0.97. The substrate employed the Arlon AD300A material with ϵ_r = 3.0 and thickness of 0.767 mm. The DCR consists of an inner closed-ring and an outer closed-ring. The unit cell of the DCR has dimensions of C_{unit} = 20 mm, L_c = 18 mm, W_{c1} = 1 mm and g_{c1} = 1 mm. The DCR is printed on a 0.8 mm-thick FR-4 substrate with a dielectric constant of 4.2.

To understand behaviours of the RMS, we take the retrieved effective parameters as representative [15], [16]. The retrieved procedure is widely used to calculate the effective parameters of MTMs. The constitutive effective parameters are obtained by using the retrieval method based on the simulated scattering parameters (S-parameters): S_{11} and S_{21}. Here, the incident electromagnetic wave is polarized with the magnetic field parallel to the resonator plane ($\boldsymbol{H}\|$ y), while the electric field polarizes along the x-axis ($\boldsymbol{E}\|$ x). Consequently, the propagation direction of wave vector $\boldsymbol{k}$ is along the z-axis (normal-incidence). Then, the simulated S-parameters were then imported into parameter extraction code, implemented in MATLAB. The complex normalized wave impedance (z) and refractive index (n) are retrieved from the S-parameters, and then effective permittivity (ϵ_{eff}) and permeability (μ_{eff}) are computed from n and z values. The magnitudes and phases of the S-parameters for DSR and DCR are shown in Fig. 2(a) and Fig. 2(b), respectively. As seen in Fig. 2, the simulated results show that the two resonant frequencies are at 1.7 GHz and 2.7 GHz for the DSR and 2.9 GHz and 5.25 GHz for the DCR. The normalized wave impedances and the retrieved parameters are shown in Fig. 3 using the simulated S-parameters plotted in Fig. 2.

Some results of the DSR loaded the MPA have been reported in [17], so in this section, we focus on the DCR one. From the retrieved parameters of the DCR as shown in Fig. 3(b), we note that the most interesting point lies in the frequency range of 2.2 GHz and 2.9 GHz (shade regions), which the permeability is close to zero. This figure confirms the obtained MNZ lying between 2.2 GHz and 2.9 GHz in operating frequency range. It can be seen that the real part of the retrieved permeability is equal to zero at 2.9 GHz and 5.5 GHz as shown in Fig. 3(b).

Besides, the zero real parts (n') of the refractive index with relatively small imaginary part are observed at three frequencies 2.9, 3.5 and 5.5 GHz. In another important point, the n' is negative over a narrow band around 3.0 GHz, dipping as low as −0.1. This type of negative n' should not be considered as DNG behaviour. In lossy materials ($n = n' + jn''$), it is possible to have the real part (n') to be negative, without having the real parts of ϵ ($\epsilon = \epsilon' + j\epsilon''$) and μ ($\mu = \mu' + j\mu''$) simultaneously negative. Because of $n' = \epsilon' z' - \epsilon'' z''$ and $z = z' + jz'' = \sqrt{\frac{\mu'\epsilon' + \mu''\epsilon''}{\epsilon^2} + j\frac{\mu''\epsilon' - \mu'\epsilon''}{\epsilon^2}}$, so it is possible to have $n' < 0$, as long as $\epsilon'' z'' > \epsilon' z'$ [18]. In addition, the frequency ranges from 3.0 GHz to 3.5 GHz and 5.5 GHz to 8.0 GHz also yield the epsilon negative medium (ENG) [19]. The use of ENG was used to reduce size [19] and enhance gain for antennas [20]. However, we focus on the range of frequency around 2.45 GHz that has the MNZ with high-ϵ medium. The effects on the use of the MNZ as a superstrate, especially on impedance bandwidth and gain enhancement, will be described in the follow section.

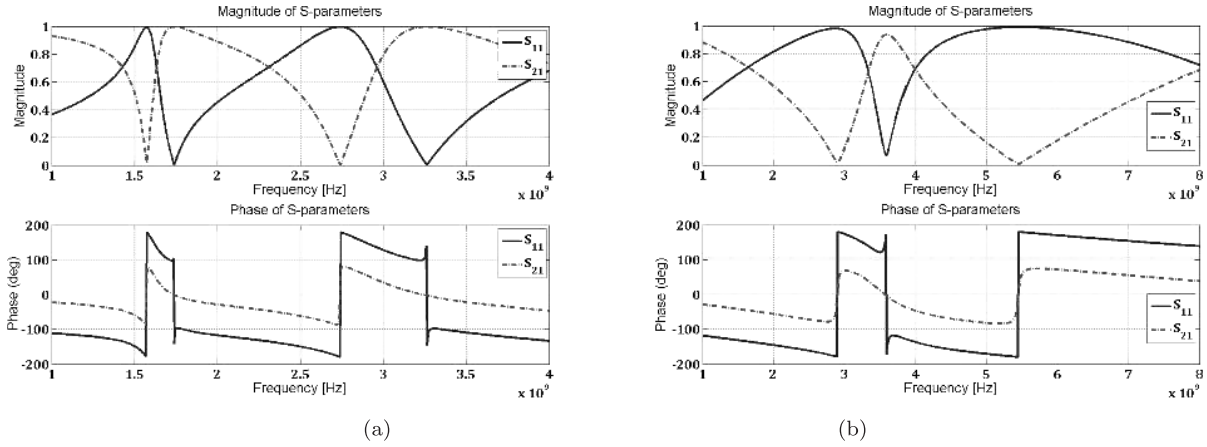

Fig. 2 Simulated magnitudes and phases of the S-parameters (S_{11} and S_{21}), (a) the double split-ring resonator (DSR) and (b) the double closed-ring resonator (DCR).

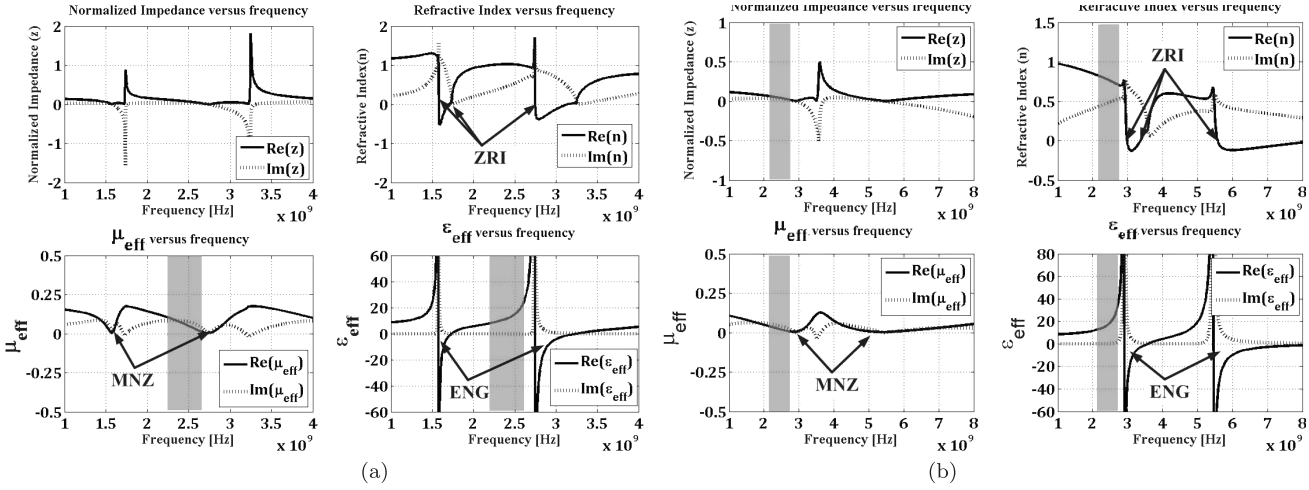

Fig. 3 The normalized wave impedance and the retrieved effective parameters of (a) the double split-ring resonator (DSR) and (b) the double closed-ring resonator (DCR).

3. Analysis of the Completed Structure

First of all, we have prepared the conventional MPA, which the central operating frequency is about 2.45 GHz. Then, we put the RMS as a superstrate to cover the MPA. For our DSR case, the MPA and the DSR dimensions were presented in the conference of ISAP2009 [17]. For DCR case, the rectangular MPA with its size of 28 mm × 29 mm ($L \times W$) is etched on a 1.6 mm thick FR-4 dielectric slab ($\epsilon_r = 4.2$). The MPA is fed by a 50-Ω coaxial probe and situated on the y-axis and is 13.5 mm (f_p) from the center as shown in Fig. 1(a). The RMS composed of the 4 × 4 DCR is suspended above the MPA.

A simple ray model can be used to describe the resonant cavity model, for a given operating frequency, the cavity height is proportional to the sum of reflection phase values associated with the RMS and the ground plane. The resonant condition is given by [21]

$$h \cong (\phi_{rms} + \phi_{gnd})\frac{\lambda_\circ}{4\pi} + \frac{\lambda_\circ}{2}N, \quad N = 0, 1, 2, ... \tag{1}$$

where ϕ_{rms} is the reflection phase of the RMS, ϕ_{gnd} is reflection phase of the ground plane, which is π for this case, $\lambda_\circ$ is the free-space wavelength and h is the cavity height. This formula assumes uniform infinite-size surfaces and ignores higher order mode coupling. By using Eq. (1), the evolution of the cavity height h versus the resonant frequency is depicted in Fig. 4. As seen, very small cavity heights ($h \ll 10$ mm) are achievable between 2.0 GHz to 3.0 GHz. At around 3.5 GHz, the cavity height is about a half-wavelength ($\lambda_0/2$) that is a conventional FPC, in which a high-gain is achieved in a narrow bandwidth. Above 3.5 GHz, the cavity actually oscillates on the second resonant mode ($N = 2$) [22]. In order to achieve a low profile and meet the resonant condition in the cavity, the summation of point at the bottom surface of the RMS should be close to zero in the operating frequency band. Theoretically, a zero cavity thickness is reached at 2.9 GHz. However, a mode jumping is observed simultaneously in the same time.

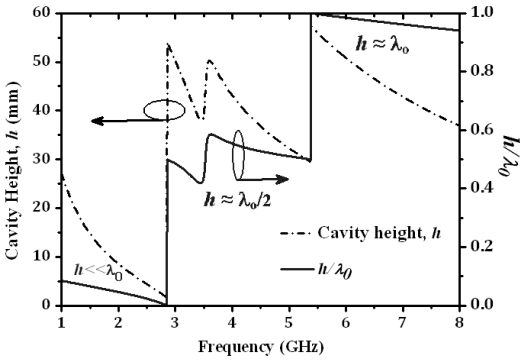

Fig. 4 The cavity height h as a function of the resonant frequency of the DCR as the RMS.

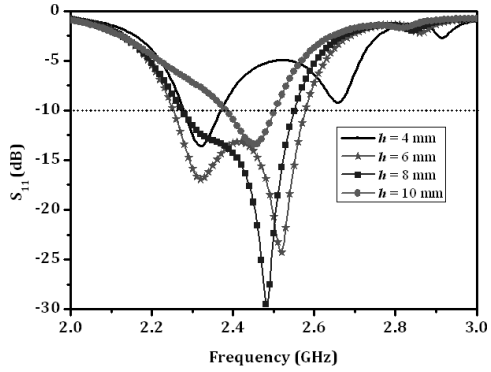

Fig. 5 Variation of S_{11} when varying the cavity height h.

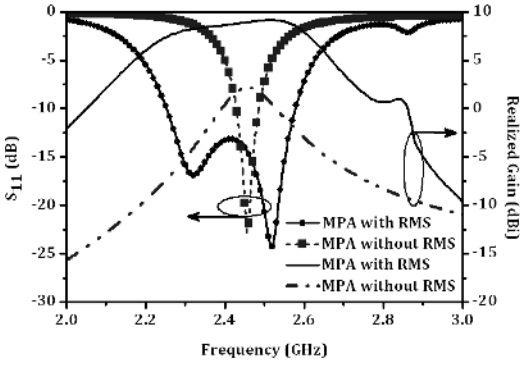

Fig. 6 Simulated return losses and realized gains of the conventional MPA-alone and the MPA with the RMS when $\epsilon_r = 4.2$ and $h = 6$ mm.

Since the cavity height (h) is small, therefore, the effects of the coupling between the RMS and the MPA on the impedance matching are studied by varying the cavity height, from 4 mm to 10 mm as shown in Fig. 5. It is seen that the highest distance of $h = 10$ mm, only a single resonant mode is excited near the resonant frequency (about 2.45 GHz) of the MPA-alone. For $h = 6$ mm and 8 mm, however, two resonant modes are excited with a good matching. In the cases of $h = 4$ mm and 10 mm, the obtained impedance bandwidths are greatly reduced and cannot meet the bandwidth requirement of the WLAN band.

The return losses and realized gains of the MPA-alone and the RMS covering the MPA are simulated and compared in Fig. 6. It is seen that for the MPA-alone, only a single resonant mode is excited with a good impedance matching. For the MPA with the RMS, however, two resonant modes at 2.32 GHz and 2.52 GHz, are excited. These two resonances are seen to be excited at frequencies in the cavity of the fundamental resonant frequency (at 2.45 GHz) of the MPA-alone due to the coupling between the MPA and the RMS. For the impedance bandwidth defined by 10-dB return loss, the MPA with the RMS provides an impedance bandwidth of 320 MHz, or 13%, which is about 5.3 times wider than the corresponding MPA-alone (60 MHz, or 2.44%). The simulated realized gain of the MPA with the RMS is shown in Fig. 6. The peak realized gain of the MPA with the RMS is about 9.77 dBi, which increases from the MPA-alone 2.3 dBi to 9.3 dBi at 2.45 GHz, which is improved observably.

The effects of the RMS covering the MPA at a small height can be considered as two folds: (*i*) parasitic loading, and (*ii*) cavity effect. The cavity effect is to put the RMS on top of a ground plane to form an FPC. The key part of the high-gain FPC antenna is its highly reflective surface. In the first frequency range of 2.0–3.2 GHz as shown in Fig. 2(b) (for DCR), the highest reflectivity occurs at 2.9 GHz. At this frequency, one can make an FPC antenna, which would have the highest directivity. However, this requires a high profile of $\lambda_\circ/2$ and exhibits a narrow bandwidth. One of the simplest ways for broadening bandwidths is to reduce cavity's Q-factor at these frequencies, where the RMS has a lower reflectivity; however, the cost is the reduction of gain and aperture efficiency. In other words, it is necessary to design the RMS with a stable reflectivity and also a phase response in a wide frequency range. In Fig. 2(b), the RMS has a magnitude difference of 0.2 and a phase difference of 20°, respectively, between 2.0 GHz and 3.0 GHz. A trade-off between high gain and wide bandwidth can be realized by properly choosing the frequency range. Hence, this frequency range is chosen because of its better frequency responses in terms of reflectivity and reflection phase. It is also called the non-resonant region [23], which is used for broadband and low-loss MTMs. Moreover, in this frequency range, both permittivity ($\epsilon'_{eff} \gg 1$) and permeability ($0 < \mu'_{eff} < 1$) are nearly constant. From the effective medium point of view, the cavity consisting of the RMS behaves as a homogeneous material with a low effective refractive index. According to Snell′s law of refraction, a low/near zero index material would make an electromagnetic wave emanates away from a primary source in any direction, to refract almost parallel to the normal of the surface of this material. This property provides a unique method of controlling the direction of emission and also the directivity enhancement. In summary, the RMS acts as a parasitic loading that increases the impedance bandwidth whereas the FPC effect enhances the gain.

The simulated radiation patterns in E- and H-planes of the MPA with and without the RMS are presented in Fig. 7.

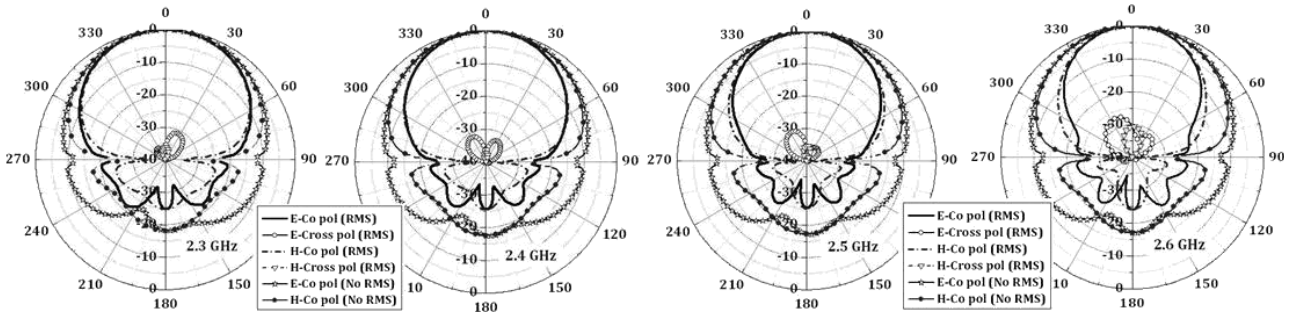

Fig. 7 Simulated radiation patterns in *y*-*z* and *x*-*z* planes at four frequencies with the 4 × 4 DCR as the RMS with $h = 6$ mm and the MPA-alone.

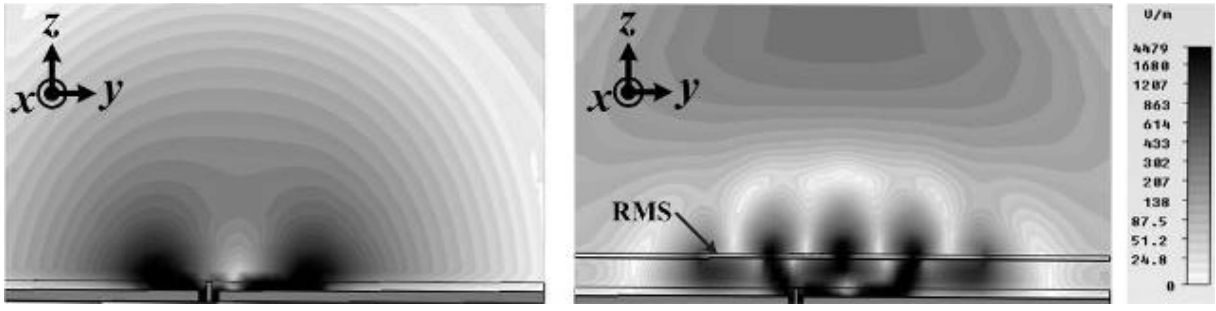

(a) (b)

Fig. 8 Vector distributions of the electric field at 2.45 GHz of antennas (a) MPA-alone and (b) MPA with the RMS.

It demonstrates the improved radiation patterns for the MPA with RMS over the MPA-alone when both are resonant and good impedance matching. The MPA with the RMS has similar radiation patterns in both the E- and H-planes. However, compared with the MPA-alone, the MPA with the RMS has the narrower lobe in both E- and H- planes. Half-power beamwidths (HPBWs) of the MPA-alone are about 82° to 86° in both E-plane ($y - z$) and H-plane ($x - z$), whereas HPBWs of the MPA with the RMS are about 45° to 73° in both E-plane ($y - z$) and H-plane ($x - z$). Thus, HPBWs of the MPA with the RMS are reduced compared with the MPA-alone. The front-to-back ratio (F/B) of the MPA with the RMS is about 27 dB over the operating frequency but the MPA-alone is only about 16 dB. In addition, the cross-polarization of the MPA with the RMS is below −30 dB for all of the operating frequency.

In order to investigate the improvement of gain by use of the RMS, the distributions of the simulated electric field at 2.45 GHz for the MPA with and without the RMS are presented in Fig. 8. It is observed that the MPA-alone has the electromagnetic wave front with a spherical wave (Fig. 8(a)) but the plane wave for the MPA with the RMS (Fig. 8(b)), which results in the increase of the antenna's gain. This means that the effective aperture is extended by adding the RMS.

4. Experiment Results and Discussion

In order to verify the simulated results, an antenna prototype

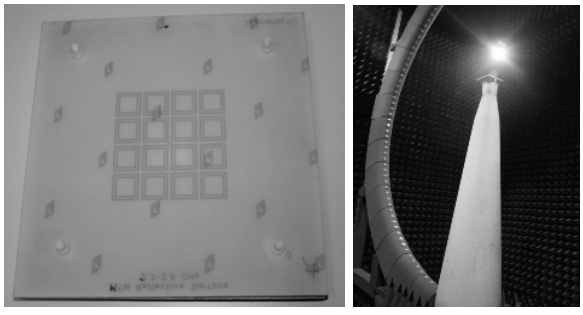

(a) (b)

Fig. 9 (a) Photograph of a prototype of the RMS and (b) the SATIMO near-field chamber.

of the 4 × 4 DCR as the RMS is fabricated and measured. The photograph of the fabricated antenna structure and the set-up for the radiation pattern measurement are illustrated in Fig. 9(a) and Fig. 9(b), respectively.

The substrate of the MPA is an FR-4 with a thickness of 1.6 mm and a dielectric constant ϵ_r of 4.2. For DCR case, it is printed on an FR-4 substrate with dielectric constant $\epsilon_r = 4.2$ and thickness of 0.8 mm. The RMS composed of the 4 × 4 DCR is placed 6 mm above the MPA. The metallic ground plane and the RMS size is 200 mm × 200 mm, corresponding to $1.63\lambda_{2.45} \times 1.63\lambda_{2.45}$, in area, where $\lambda_{2.45}$ is the free-space wavelength at 2.45 GHz. The RMS is supported by four plastic posts.

The S_{11} obtained from simulation and measurement

of the MPA with the RMS with a very good agreement is shown in Fig. 10. It is clearly seen that two resonant modes at 2.32 GHz and 2.6 GHz are excited with good impedance matching. These two modes together give an impedance bandwidth of 350 MHz, or about 13% (from 2.30 GHz to 2.65 GHz) while the bandwidth of the matched MPA-alone is about 2.4%. The S_{11} of the 4×4 DCR as the RMS with various permittivity values are also plotted in Fig. 10. The permittivity is increased, the resonant frequency decreases. From this figure, the measured result of S_{11} is close to the ϵ_r = 4.2.

Figures 11 and 12 show the measured far-field radiation patterns in the anechoic chamber at the Chinese University of Hong Kong. Very good broadside radiation patterns are observed and the cross-polarization in the principal planes is seen to be less than −29 dB especially for the $y - z$ plane. The front-to-back ratios (F/B) were also measured. From measured results, the F/B is more than 27 dB for all the operating frequency. In addition, the realized gains of the MPA with and without the RMS were measured as shown in Fig. 13. The gain for the MPA-alone is 2.3 dBi, whereas the MPA with the RMS can increase to 9.3 dBi at its center frequency. An improvement in the gain of 7 dB has been obtained. Moreover, the realized gains of the MPA with the RMS are all improved within the operation bandwidth. Gen-

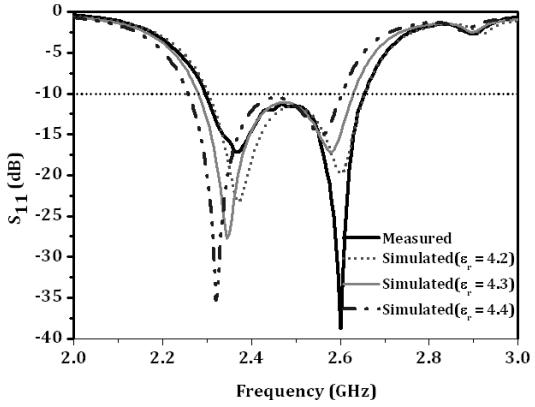

Fig. 10 Simulated and measured S_{11} of the 4×4 DCR as the RMS with different ϵ_r when h = 6 mm.

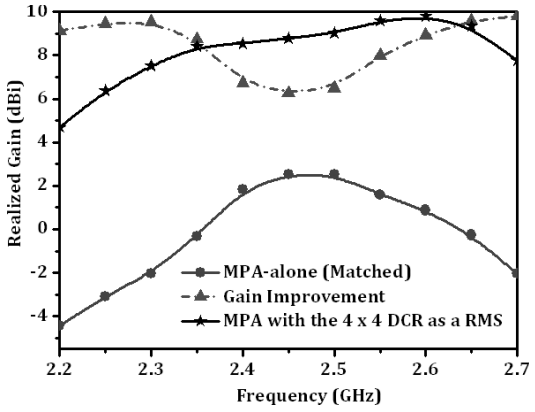

Fig. 13 Comparison of realized gains from measurement between the MPA with the 4×4 DCR as the RMS and the MPA-alone with a good matching.

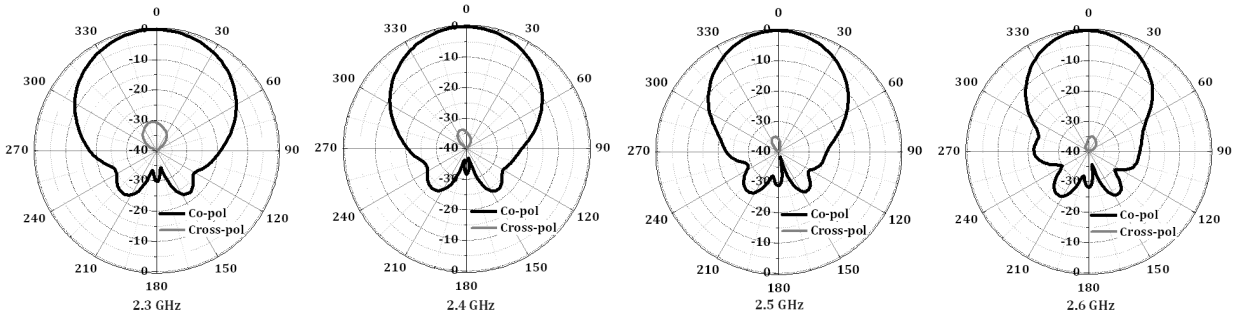

Fig. 11 Measured radiation patterns in E-plane (*y-z plane*) at four frequencies with the 4×4 DCR as the RMS when h = 6 mm.

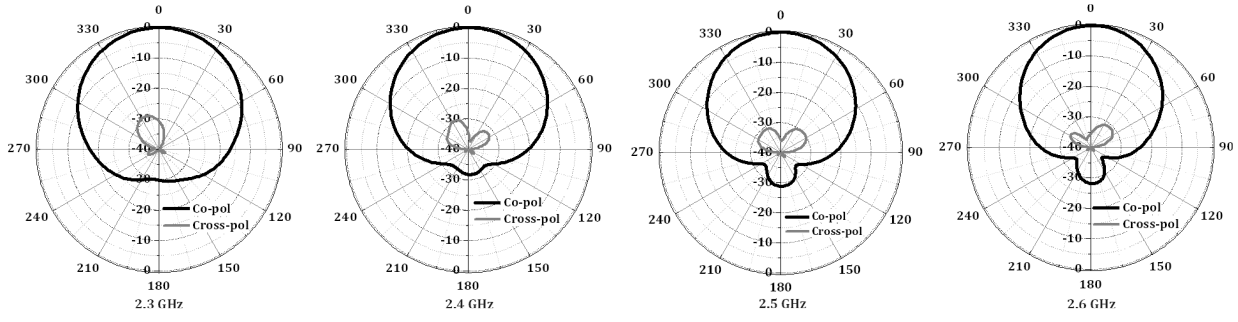

Fig. 12 Measured radiation patterns in H- plane (*x-z plane*) at four frequencies with the 4×4 DCR as the RMS when h = 6 mm.

Table 1 Measured antenna performances of three antenna configurations.

Antenna Types	BW@−10 dB (MHz, %)	Front-to-back ratio (dB)	Maximum Gain (dBi)	Cross-polar (dB)
MPA-alone	60, 2.44	15–18	2.31	15–40
MPA+DSR-RMS [17]	130, 5.23	15–20	9.16	20–45
MPA+DCR-RMS	320, 13.0	27–35	9.77	29–50

erally speaking, the realized gains of the antenna with the RMS have an about 7 dB enhancement in comparison with the MPA-alone.

The 3-dB gain bandwidth is 13% from 2.3 GHz to 2.6 GHz, which is also much wider than that of the antenna without the RMS and with the 4×4 DSR as the RMS [17]. Compared with [24], which is designed at the same center frequency (2.45 GHz) and the same ground plane size (200 mm × 200 mm), our antenna has wider impedance and gain bandwidths. Antenna performances of the three different configurations, the MPA-alone, the MPA with the 4×4 DSR as the RMS and the MPA with the 4×4 DCR as the RMS, are tabulated in Table 1.

5. Conclusion

In this paper, the use of the reflective metasurface (RMS) as a superstrate for impedance bandwidth and gain enhancement of the microstrip patch antenna has been presented. The DSR and DCR arrays have been used as the RMS. Since the sum of the RMS reflection phase and the ground plane is closed to zero, the cavity height can be reduced without using an AMC as the ground plane. The RMS is designed based on the mu-near-zero (MNZ) and the high epsilon properties, which are considered as the MPA of gain enhancement. The proximity EM coupling of the RMS is regarded as the MPA for bandwidths enhancement.

Acknowledgement

The authors would like to thank the Microwave and Wireless Communication Laboratory of the Chinese University of Hong Kong, for assistance in the antenna measurements.

References

[1] K.-L. Wong, Compact and Broadband Microstrip Antennas, John Wiley & Sons, New York, 2002.
[2] K.J. Vinoy, K.A. Jose, V.K. Varadanm, and V.V. Varadan, "Gain enhanced electronically tunable microstrip patch antenna," Microw. Opt. Technol. Lett., vol.23, no.6, pp.368–370, Dec. 1999.
[3] D.R. Jackson and N.G. Alexopoulos, "Gain enhancement methods for printed-circuit antennas," IEEE Trans. Antennas Propag., vol.AP-33, no.9, pp.976–987, Jan. 1985.
[4] N. Guerin, S. Enoch, G. Tayeb, P. Sabouroux, P. Vincent, and H. Legay, "A metallic Fabry-Perot directive antenna," IEEE Trans. Antennas Propag., vol.54, no.1, pp.220–224, Jan. 2006.
[5] J. Ju, D. Kim, and J. Choi, "Fabry-Perot cavity antenna with lateral metallic walls for WiBro base station applications," Electron. Lett., vol.45, no.3, pp.141–142, Jan. 2009.
[6] R. Sauleau, P. Coquet, T. Matsui, and J.-P. Daniel, "A new concept of focusing antennas using plane-parallel Fabry-Perot cavities with nonuniform mirrors," IEEE Trans. Antennas Propag., vol.51, no.11, pp.3171–3175, Nov. 2003.
[7] A.P. Feresidis, G. Goussetis, S. Wang, and J.C. Vadaxoglou, "Artificial magnetic conductor surface and their application to low-profile high-gain planar antenna," IEEE Trans. Antennas Propag., vol.53, no.1, pp.209–215, Jan. 2005.
[8] A. Foroozesh and L. Shafar, "Application of combined electric — and magnetic — conductor ground planes for antenna performance enhancement," Canadian J. of Elec. and Com. Eng., vol.33, no.2, pp.87–98, 2008.
[9] A. Alu, N. Engheta, A. Erentok, and R.W. Ziolkowski, "Single-negative, double-negative, and low-index metamaterials and their electromagnetic applications," IEEE Antennas Propag. Mag., vol.49, no.1, pp.23–36, Feb. 2007.
[10] J. Ju, D. Kim, W.J. Lee, and J.I. Choi, "Wideband high-gain antenna using metamaterial superstrate with the zero refractive index," Microw. Opt. Technol. Lett., vol.51, no.9, pp.1973–1976, Aug. 2009.
[11] H. Zhou, Z. Pei, S. Qu, S. Zhang, J. Wang, Z. Duan, H. Ma, and Z. Xu, "A novel high-directivity microstrip patch antenna based on zero-index metamaterial," IEEE Antennas and Wirel Prog. Lett., vol.8, pp.538–541, 2009.
[12] S. Enoch, G. Tayeb, P. Sabouroux, N. Guerin, and P. Vincent, "A metamaterial for directive emission," Phys. Rev. Lett., vol.89, no.21, pp.2139021–2139024, Nov. 2002.
[13] IE3D Simulator, Zeland Software, 1997.
[14] CST Microwave Studio, CST GmbH, Darmstadt, Germany.
[15] H. Chen, B.I. Wu, L. Ran, T.M. Grzegorczyk, and J.A. Kong, "Robust method to retrieve the constitutive effective parameters of metamaterials," Phys. Rev. E, vol.70, pp.016608–0166015, 2004.
[16] D.R. Smith, D.C. Vier, T. Koschny, and C.M. Soukoulis, "Electromagnetic parameter retrieval from inhomogeneous metamaterial," Phys. Rev. E, vol.71, pp.036617–036618, 2005.
[17] S. Chaimool, K.L. Chung, and P. Akkaraekthalin, "A 2.45 GHz WLAN high-gain antenna using a metamaterial reflecting surface," Proc. ISAP2009, Bangkok, Thailand.
[18] J. Zhou, T. Koschny, L. Zhang, G. Tuttle, and C.M. Soukoulis, "Experimental demonstration of negative index of refraction," Appl. Phys. Lett., vol.88, no.22, 221103, 2006.
[19] Y. Lee and Y. Hao, "Characterization of microstrip patch antennas on metamaterial substrates loaded with complementary split-ring resonators," Microw. Opt. Technol. Lett., vol.50, no.8, pp.2131–2135, Aug. 2008.
[20] Y. Liu and X. Zhao, "Enhance patch antenna performances using dendritic structure metamaterials," Microw. Opt. Technol. Lett., vol.51, no.7, pp.1732–1738, July 2009.
[21] A.P. Feresidis and J.C. Vardaxoglou, "High gain planar antenna using optimised partially reflective surfaces," IEE Proc. Microw. Antennas Propag., vol.148, no.6, pp.345–350, Dec. 2001.
[22] A. Ourir, A. de Lustrac, and J.-M. Lourtioz, "All-metamaterial-based subwavelength cavities (λ/60) for ultrathin directive antennas," Appl. Phys. Lett., vol.88, 0841031, 2006.
[23] R. Liu, Q. Cheng, T.J. Cui, and D.R. Smith, Broadband and low-loss non-resonant metamaterials in Chapter 5, Metamaterials, Theory, Design and applications, Springer, New York Dordrecht Heidelberg London, 2010.
[24] S.N. Burokur, A. Ourir, J.-P. Daniel, P. Ratajczak, and A. de Lustrac, "Highly directive ISM band cavity antenna using a bi-layered metasurface reflector," Microw. Opt. Technol. Lett., vol.51,

no.6, pp.1393–1396, June 2009.

Sarawuth Chaimool received the B.Eng. M.Eng. and the Ph.D. degrees in Electrical Engineering from King Mongkut University of Technology, North Bangkok (KMUTNB), Thailand, in 2001, 2003 and 2008, respectively. In 2004, he joined the Department of Electrical Engineering, KMUTNB, as an instructor. His current research interests include bandpass filters, metamaterials and planar antennas.

Kwok L. Chung received his B.E. degree with first-class honours and his Ph.D. degree in Electrical Engineering from the University of Technology, Sydney (UTS), Australia. In 2000, he received the Australian Postgraduate Award from the Commonwealth Department of Education, Science and Training (DEST), Australia. Before he moved to Australia, he was a Technical and Distribution Manager at the Telemecanique Asia Pacific Ltd., Hong Kong from 1987 to 1993. Since 2000, he has been a researcher in the Cooperative Research Centre for Satellite Systems (CRCSS) at UTS. In 2004, he became a Lecturer at the Faculty of Engineering, UTS. He returned to Hong Kong in 2006, and joined the Department of Electronic and Information Engineering, Hong Kong Polytechnic University, as a Lecturer. His current research interests include metamaterial antennas, circularly polarized antennas and arrays, wideband, multi-band printed antennas, the applications of evolutionary algorithms for microwave components and antennas design. Dr. Chung is a senior member of IEEE, AP and MTT Societies. He currently serves as the Honorary Vice Chairman for the IEEE AP/MTT Hong Kong Joint Chapter.

Prayoot Akkaraekthalin received the B.Eng. and M.Eng. degrees in Electrical Engineering from King Mongkut University of Technology, North Bangkok (KMUTNB), Thailand, in 1986 and 1990, respectively, and the Ph.D. degree in Electrical Engineering from the University of Delaware, Newark, USA, in 1998. From 1986 to 1988, he worked in the Microtek Laboratory, Thailand, as a Research and Development Engineer. In 1988, he joined the Department of Electrical Engineering, KMUTNB, as an instructor. His research interests are in the areas of microwave circuit design, optoelectronics, and telecommunications.